Journal of Organometallic Chemistry 925 (2020) 121466

Contents lists available at ScienceDirect

Journal of Organometallic Chemistry

journal homepage: www.elsevier.com/locate/jorganchem

Synthesis and structure of annulated dithieno[2,3-*b*;3′,2′-*d*]thienyl- and ring-opened 3,3′-bithienyl Fischer carbene complexes

Zandria Lamprecht [a], Frederick P. Malan [a], David C. Liles [a], Simon Lotz [a], Daniela I. Bezuidenhout [b,*]

[a] Department of Chemistry, University of Pretoria, Private Bag X20, Hatfield, 0028, Pretoria, South Africa
[b] Laboratory of Inorganic Chemistry, Environmental and Chemical Engineering, University of Oulu, P. O. Box 3000, 90014, Oulu, Finland

ARTICLE INFO

Article history:
Received 15 July 2020
Revised 2 August 2020
Accepted 9 August 2020
Available online 11 August 2020

Keywords:
Annulated thiophene
Fischer carbene complexes
Group 6 transition metals
Dihydrodesulphurization

ABSTRACT

Nucleophilic attack on the central sulphur of dithieno[2,3-*b*;3′,2′-*d*]thiophene (DTT) by *n*-BuLi opens the central thiophene ring and afforded, after subsequent reaction with $Cr(CO)_6$ and alkylation with $[Et_3O][BF_4]$, a series of mono- and biscarbene complexes containing a 3,3′-dithienyl backbone with a SBu substituent. Repeating the reaction with diisopropylamine as the nucleophile, leads to a dihydrodesulphurization reaction with ring-opening of the central thiophene ring of DTT and elimination of the sulphur atom. Subsequent reaction with *n*-BuLi or LDA, $Cr(CO)_6$ and $[Et_3O][BF_4]$ afforded 3,3′-dithienyl mono- and biscarbene complexes. In both instances α,α'-dithienothiophene biscarbene complex was observed spectroscopically but not isolated. By using α,α'-dibromodithieno[2,3-*b*;3′,2′]thiophene as substrate, improved yields of the targeted mono- and biscarbene complexes of [2,3-*b*;3′,2′-*d*]-DTT (M=Cr, W) could be obtained. The biscarbene complexes were unstable in the reaction mixture but in the case of tungsten could be isolated after *in situ* aminolysis with dimethylamine. The use of KHMDS as base converted $Cr(CO)_6$ to $K[Cr(CO)_5(CN)]$ and after reaction with DTT and subsequent alkylation with $[Et_3O][BF_4]$, afforded the chromium tetracarbonyl carbene complex of DTT.

1. Introduction

Compared to chain structures of α,α'-oligo- and polythiophenes, planar condensed thiophenes display more efficient and extended π-conjugation, better p-orbital overlap, improved charge transfer properties and higher chemical stability [1]. α- and β-annulated oligothiophenes, specifically dithienothiophene (DTT) derivatives have already been developed as promising semiconducting materials, organic conductors, photosensitive materials and light emitting devices [2–7].

The preparation of annulated thiophenes is challenging and examples in organometallic chemistry are therefore limited. When considering annulated thiophenes as precursors for organometallic compounds, stability factors need to be taken into account [8,9]. Derivatives of the six possible constitutional isomers of DTT are planar, electron excessive, π-conjugated and aromatic. [3,2-*b*;2′,3′-*d*]-DTT with the sulphur atoms in relative orientations *up-down-up*, displays a linear conjugated pathway throughout the molecule, allowing communication between the α-positions without involving the sulphur atoms. A conjugation system from S1 to S3 is also possible in [3,2-*b*;2′,3′-*d*]-DTT. A linear conjugated pathway through [2,3-*b*;3′,2′-*d*]-DTT, another isomer, is made impossible by the central cross-conjugated double bonds (sulphur atoms orientated on the same side of the ring, *up-up-up*). A molecular orbital approach for the overlapping of p-orbitals gives a better picture of electron delocalization of π-bonds (Fig. 1). The reactivity of [3,2-*b*;2′,3′-*d*]-DTT and [2,3-*b*;3′,2′-*d*]-DTT was investigated by means of their protiodetritiation reactions [10,11]. Partial rate factors were calculated which represent how fast the tritium, in each position on the heteroarenes, exchanges with a proton (Fig. 1), as a ratio to benzene's detritiation rate. The α-positions are in each case more reactive than the β-positions, with the reactivity of [2,3-*b*;3′,2′-*d*]-DTT > [3,2-*b*;2′,3′-*d*]-DTT.

The combination of an electron-rich condensed thiophene substituent with an electron-deficient Fischer carbene carbon can result in an anticipated "push-pull" or polarizing electronic situation. Carbene complexes of DTT derivatives are rare, and only group 6 transition metal mono- and biscarbene complexes of the [3,2-*b*;2′,3′-*d*]-DTT isomer are known [12–15]. In these examples (Fig. 2), the lithiation reactions were performed in hexane and both the mono- and biscarbene complexes could be isolated in reason-

* Corresponding author.
E-mail address: daniela.bezuidenhout@oulu.fi (D.I. Bezuidenhout).

https://doi.org/10.1016/j.jorganchem.2020.121466

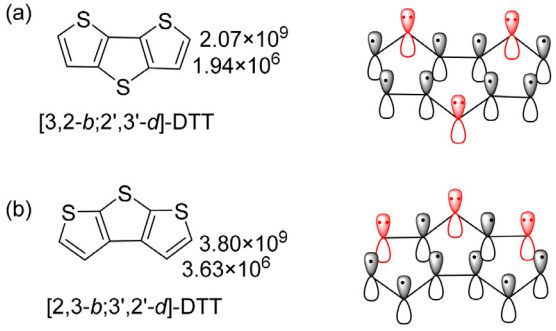

Fig. 1. Comparison of π-conjugated pathways in [3,2-*b*;2′,3′-*d*]-DTT and [2,3-*b*;3′,2′-*d*]-DTT from atomic p_π orbital perspective and partial rate factors (α- and β-positions) for detritiation.[10,11].

able yields (>30%). The complexes are stable in the solid state, but the biscarbene complexes to a lesser extent in solution. The latter were readily oxidized to the carbene-ester complex by trace amounts of oxygen, and at elevated temperature a carbene-carbene coupled biscarbene complex with an extended conjugated linker formed. Notably, in all instances the [3,2-*b*;2′,3′-*d*]-DTT rings remained intact (inert) during carbene formation reactions and subsequent reactions occurred only at the carbene sites.

In this study, [2,3-*b*;3′,2′-*d*]-DTT is chosen as precursor for the preparation of Fischer carbene complexes (FCCs) and is compared with results obtained for the [3,2-*b*;2′,3′-*d*]-DTT isomer. The role of different bases as well as the reactivity patterns during lithiation and carbene formation are studied to expand the scope of possible reactions with DTT in the context of Fischer carbene chemistry.

2. Results and discussions

2.1. Syntheses of precursors and complexes

The precursor [2,3-*b*;3′,2′-*d*]-DTT (**P1**) was prepared as described by Nenajdenko [3], with amendments as suggested by Allared [16]. The authenticity and purity of **P1** were determined by spectroscopic characterization (Fig. S1, Supplementary data). Carbene complexes were prepared by making use of **P1** in three different methods by using a range of strong bases: *n*-BuLi (*n*-butyllithium), a mixture of nucleophilic diisopropylamine (HDA) and *n*-BuLi (with subsequent formation of lithium diisopropylamide (LDA)), and potassium bis(trimethylsilyl)amide (KHMDS) (non-nucleophilic base). Reactions were performed at low temperatures (−78°C) to create the opportunity to discriminate between reaction sites. As a measure of favoured reaction sites and stabilities of reaction intermediates, the yields and compositions of the final isolated carbene complexes serve as indicators. To further activate **P1** and direct reactions to the α-positions of the DTT substrate the α-protons were exchanged by bromo substituents to facilitate lithium-halogen exchange reactions. Brominating the α-positions using NBS produces 5,5′-dibromo-[2,3-*b*;3′,2′-*d*]-DTT (**P2**), as an excellent building block to be used in Fischer carbene synthesis [3]. Two further experiments were executed with the aim to protect the DTT ring and to stabilize final reaction products (Scheme 1).

Method 1 comprises of the classical Fischer method using *n*-BuLi, in THF at low temperatures (−78°C), (Scheme 1, method 1) [17]. The main reaction pathway involves a ring opening reaction of the central thiophene ring in **P1** leading to the formation of a 3,3′-bithienyl-2-SBu backbone [18,19]. In a proposed sequence of reactions, the base (Bu^-) participates in nucleophilic attack on the central sulphur atom of the three fused thiophene rings, breaking open the central thiophene ring of **P1** (Scheme 2). After opening the central ring, an anion resides on an α-position of the adjacent ring (2′ position). Subsequent reaction with the metal carbonyl and alkylation will afford the monocarbene complex with both substituents on inside ring positions on separate rings, [2′-SBu-C_4H_2S-3,3′-{2-C(OEt)$Cr(CO)_5$}C_4H_2S] (**2**). The anion is transferable to other active α-positions. The most active one is the remaining α-position (5) of the thiophene ring with the SBu substituent. We anticipate that conversion of the anion site to the remaining α-position on the thiophene bearing the SBu substituent is favoured. The activation is enhanced at this site by the presence of the SBu substituent in the other α-position of the same ring. After alkylation the product isolated is [{2-SBu,5-C(OEt)$Cr(CO)_5$}C_4HS-3,3′-C_4H_3S] (**1**) which represents the major product of the reaction. The next most active site for biscarbene complex formation will be at an inside α-position (2′) of the second thiophene ring. The biscarbene complex that formed after alkylation has the second highest yield, and is [{2-SBu,5-C(OEt)$Cr(CO)_5$}C_4HS-3,3-{2′-C(OEt)$Cr(CO)_5$)}C_4H_2S] (**3**). The second biscarbene complex of 3,3′-bithienyl-2-SBu is isolated in a very low yield and displays a second carbene substituent in the outside position (5′) of the second thiophene ring, [{2-SBu,5-C(OEt)$(Cr(CO)_5$}C_4HS-3,3′-{5′-C(OEt)$Cr(CO)_5$}C_4H_2S] (**4**). The formation of the second carbene group in the electronically favoured inside position (**3**), is in competition with formation at the second outside α-position (**4**), which is sterically the less crowded position. The byproduct butylcarbene complex make up the remainder of complexes obtained by method 1. The targeted biscarbene complex [{$Cr(CO)_5$C(OEt)}$_2$-5,5′-$C_8H_2S_3$] (**5**) was spectroscopically identified as present in the reaction mixture in trace amounts, but could not be isolated.

Mono- and dinuclear complexes are obtained by using 1.8 equivalents of the lithiating agent to one equivalent of **P1**. The stoichiometric ratio employed was rationalized as 1.5 molar equivalents are required for the formation of a 1:1 ratio of mono-:biscarbene products, with 1.2 equivalents excess. Nucleophilic attack of the mono- and dianions on carbonyl carbon atoms of chromium hexacarbonyl occur upon their addition. Quenching the resulting acylmetallates with [Et_3O][BF_4] yielded the neutral carbene compounds. Monocarbene complexes **1** (yield 32%) and **2** (yield 8%) along with biscarbene complexes **3** (yield 24%), **4** (yield <3%) and **5** (yield <3%) were obtained. As major products, **1** and **3** prove intra-ring electron delocalization from C2 (SBu) to C5 stabilizes the carbene fragment on C5. In the case of **3**, additional interring stabilization from C2 to C2′ allows a second carbene fragment to coordinate to C2′.

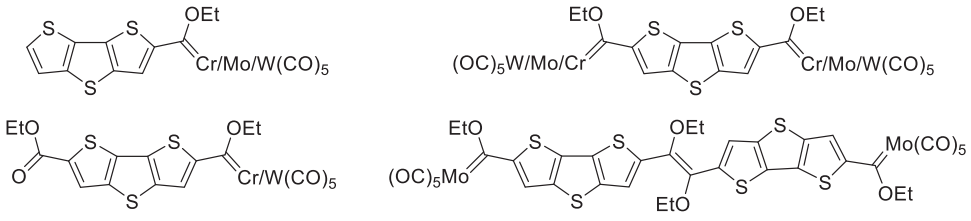

Fig. 2. Known [3,2-*b*;2′,3′-*d*]-DTT carbene complexes [12–15].

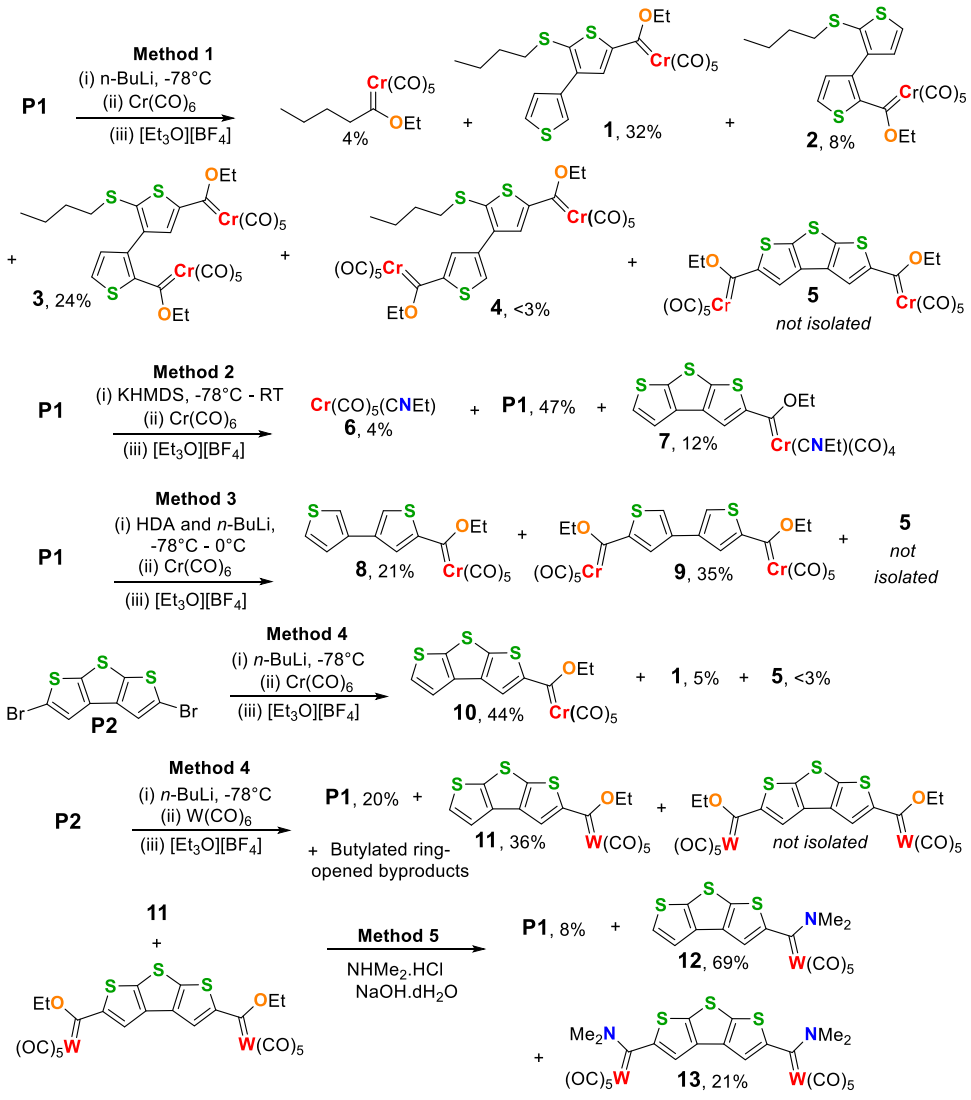

Scheme 1. Syntheses of Fischer carbene complexes containing 3,3′-bithienyl-2-SBu, 3,3′-bithienylene (BT) and [2,3-*b*;3′,2′-*d*]-DTT substituents by applying different methodologies.

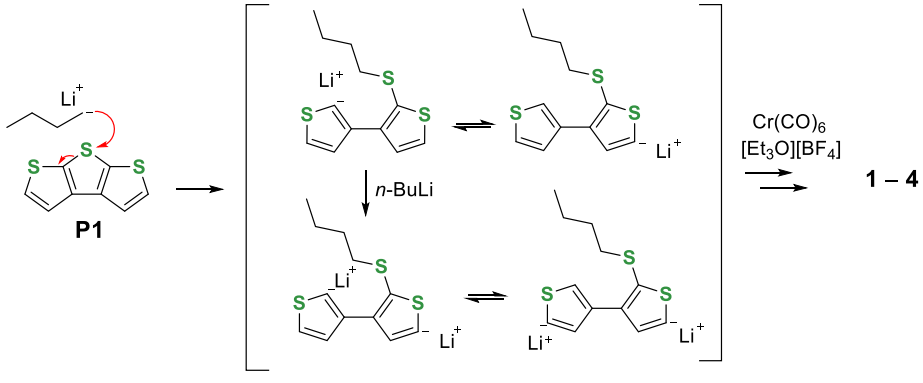

Scheme 2. Proposed reaction pathway of nucleophilic attack by *n*-BuLi on **P1**.

Method 2 (Scheme 1) involves the deprotonation of **P1** using 2.4 equivalents KHMDS (2 equivalents including 1.2 times excess, allowing for dinuclear biscarbene formation), with the rest of the reaction following the classical Fischer method. The reaction proceeded poorly as 47% of the starting material was recovered and only little evidence of deprotonation was observed with the formation of [Cr(CO)$_4${C(OEt)-5-C$_8$H$_3$S$_3$}CNEt] (**7**, yield 12%). Hence the amide base also attacked carbonyl groups as is evident from the formation of **7** and [Cr(CO)$_5$(CNEt)] (**6**, yield 4%), after alkylating with Meerwein's salt [Et$_3$O][BF$_4$] [20]. A proposed mecha-

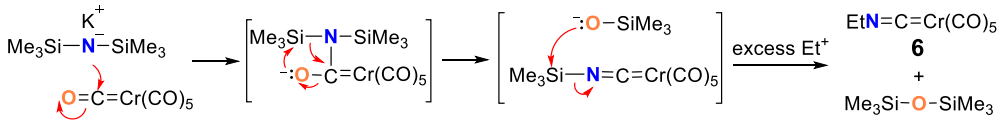

Scheme 3. Proposed mechanism of the reaction of KHMDS with $Cr(CO)_6$ to form **6**.

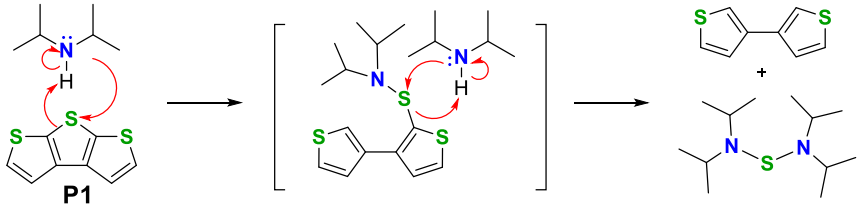

Scheme 4. Proposed reaction pathway of dihydrodesulphurization of **P1** by HDA.

nism shows the base acting as a nucleophile and nucleophilic addition occurs to the carbonyl carbon atom of chromium hexacarbonyl producing $K[Cr(CO)_5CN]$ (Scheme 3). The latter reacts with deprotonated **P1** to afford **7**, while unreacted cyanide of $[Cr(CO)_5CN]^-$ is alkylated to give **6** (Scheme 3).

Nucleophilic attack on (and ring-opening of) **P1** with the use of *n*-BuLi was unexpected and is not observed for the reaction of *n*-BuLi on the isomer of **P1**, [3,2-*b*;2′,3′-*d*]-DTT), or other annulated thiophenes [12–15,21]. The reaction is unique for **P1** (three sulphurs on the same side of DTT) and might be ascribed to the lack of conjugated pathways from the two ends of **P1** to the central sulphur atom (now more electrophilic). Hence an experiment was planned to compare the rates of nucleophilic attack and deprotonation by using a stronger nucleophile (*e.g.* amine, in this case diisopropylamine HDA) along with *n*-BuLi (Scheme 1, method 3). In the reaction, 2.4 equivalents of HDA and *n*-BuLi (2 equivalents to allow for dinuclear complex formation with 1.2 times excess) were used. At very low temperatures (*ca.* −80 °C), HDA remains protonated, and *n*-BuLi unreacted. The occurrence of nucleophilic attack on the central sulphur atom of **P1** by HDA can therefore be compared to the probability of nucleophilic attack by the stronger base/weaker nucleophile, *n*-BuLi. As the temperature of the reaction mixture is allowed to increase gradually, LDA is generated *in situ* (deprotonation of HDA by *n*-BuLi), and either LDA or excess remaining *n*-BuLi can deprotonate **P1**. It was determined that the first reaction was the nucleophilic attack of HDA on the central sulphur atom of **P1**, leading first to ring-opening and after a second attack, to dihydrodesulphurization of **P1**. Thus a route that yields $S(DA)_2$ (DA = diisopropylamide) along with 3,3′-bithiophene (3,3′-BT) is proposed (Scheme 4). A more reactive and electrophilic central sulphur initialises the first addition of HDA, resulting in an intermediate with favourable electronic properties facilitated by the external thiophene rings, allowing for a second attack with elimination of the sulphur atom.

Subsequent reaction (deprotonation) of the *in situ* generated 3,3′-BT with *n*-BuLi or formed LDA, followed the classical Fischer method. The mono- and biscarbene complexes of 3,3′-BT, [{5-C(OEt)$Cr(CO)_5$)C_4H_2S}-3,3′-C_4H_3S] (**8**, yield 21%) and [5,5′-{$Cr(CO)_5C(OEt)$}$_2$-3,3′-$C_8H_4S_2$] (**9**, yield 35%) respectively, were previously synthesized from 3,3′-BT and have been published [22]. Spectroscopic evidence for the formation of trace amounts of the DTT biscarbene complex **5** was seen in the reaction mixture, as for method 1.

Bromination of the α-positions of DTT produces 5,5′-dibromo-[2,3-*b*;3′,2′-*d*]-DTT (**P2**) (see Fig. S1 for NMR characterization),

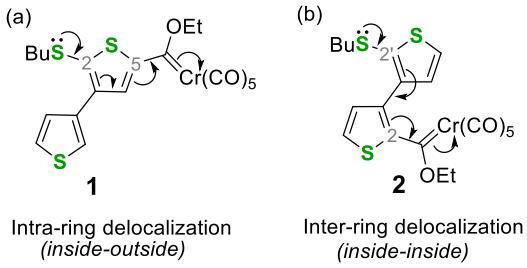

Fig. 3. Electron delocalization in **1** and **2**.

which is an excellent building block to be used in Fischer carbene synthesis, as lithium-halide exchange reactions show many advantages compared to deprotonation reactions in annulated thiophene substrates. The double lithium-halogen exchange reaction affords the debromination of **P2** using 2.4 equivalents *n*-BuLi (Scheme 1, method 4) and subsequent reaction with the metal carbonyl and alkylating agent lead to the targeted compounds [$Cr(CO)_5${C(OEt)-5-$C_8H_3S_3$}] (**10**, yield 44%) and **5** (trace amount). Deprotonation (**10**) is in competition with ring-opening (**1**). Compound **1** (5% yield) was observed as by-product of the reaction. Repeating the reaction with tungsten carbonyl gave no ring-opening products but [$W(CO)_5${C(OEt)-5-$C_8H_3S_3$}] (**11**, yield 36%), and the corresponding biscarbene complex [{$W(CO)_5C(OEt)$}$_2$-5,5′-$C_8H_2S_3$] in very low yield (not purified/isolated), as well as 20% **P1** (debrominated **P2**). During work-up it was observed that **P2** readily converts to **P1**. The biscarbene complex **5** could be isolated (Scheme 1), but the low yield allowed only for characterization by ^{1}H NMR and FT-IR spectroscopy, as well as single crystal analysis. The tungsten analogue (method 4), could not be isolated, leading to the conclusion that the bisethoxycarbene complexes are highly reactive in the reaction mixtures in solution. Method 5 (Scheme 1) was therefore introduced to stabilize the biscarbene complexes before purification and isolation, and applied to the more reactive tungsten complexes. The mono- and bisethoxycarbene tungsten complexes are first synthesized using method 4, followed by *in situ* aminolysis of the reaction mixture. Excess dimethylamine hydrochloride and sodium hydroxide are added to the reaction mixture. Thereafter, distilled H_2O was added dropwise until all the suspended salts dissolved and reacted [23]. [$W(CO)_5${C(NMe_2)-5-$C_8H_3S_3$}] (**12**, yield 69%) and [{$W(CO)_5C(NMe_2)$}$_2$-5,5′-$C_8H_2S_3$] (**13**, yield 21%) were isolated in moderate to good yields along with 8% of **P1**.

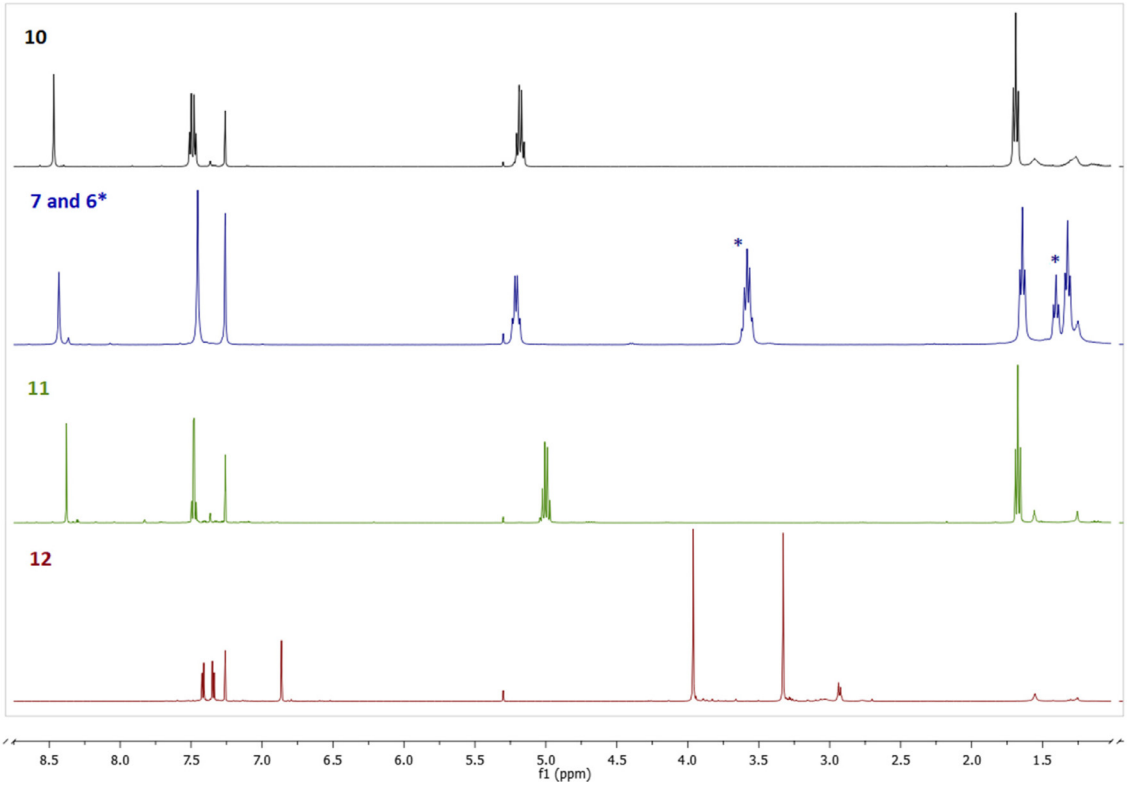

Fig. 4. ^{1}H NMR spectra showing chemical shift patterns for **7**, **10**–**12**.

Table 1
^{1}H NMR chemical shifts (δ) of the carbene complexes.

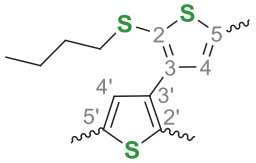

1, 3, 4

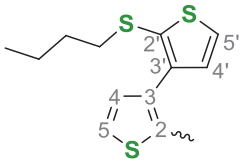

2

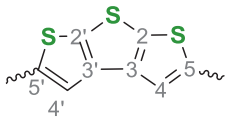

5, 7, 10-13

Complex	H4	H5	H2′	H4′	H5′	SBu[a]	OEt[b]	NEt/NMe$_2$[c]
1	8.28		7.58	7.40	7.42	3.08, 1.76, 1.50, 0.96	5.13, 1.67	
2	7.04	7.72		6.84	7.30	2.58, 1.41, 1.25, 0.80	4.84, 1.07	
3	8.01			6.99	7.79	2.97, 1.68, 1.41, 0.93	C5: 5.15, 1.68 C2′: 4.91, 1.14	
4	8.32		7.90	8.58		3.12, 1.78, 1.50, 0.98	C5: 5.16, 1.67 C5′: 5.24, 1.71	
5	8.49						5.21, 1.71	
7	8.43			7.45	7.45		5.21, 1.64	3.57, 1.32
10	8.47			7.50	7.47		5.18, 1.69	
11	8.38			7.49	7.47		5.00, 1.67	
12	6.86			7.34	7.42			3.96, 3.33
13	6.82							3.96, 3.35

[a]Proton chemical shifts for the $SCH_2CH_2CH_2CH_3$ fragment are reported with the first value being the chemical shift of the first methylene group after the sulphur atom, followed by the values of the second and third methylene groups. The last chemical shift is that of the methyl group.
[b]Proton chemical shifts for the ethoxy fragment are reported with the first value being the chemical shift of the methylene group, and the second the chemical shift of the methyl group.
[c]Proton chemical shifts for the NEt fragment (**7**) are reported with the first value being the chemical shift of the methylene group, and the second the chemical shift of the methyl group. In the case of **12** and **13** the chemical shifts represent the methyl groups of NMe_2.

2.2. Spectroscopic characterization

2.2.1. ^{1}H NMR spectroscopy

NMR spectra, recorded in $CDCl_3$, support the assigned molecular structures of the compounds. ^{1}H NMR data are summarized in Table 1. Two classes of monocarbene complexes (**1** (C5-) and **2** (C2-)) were isolated from method 1 (Scheme 1) containing a 3,3′-BT-2-SBu- and 3,3′-BT-2′-SBu-thienyl substituent, respectively. Both SBu (*inside*) and the carbene substituent (*outside*) are on the same thiophene ring in **1**, while both substituents are on the 'inside' position on different thiophene rings in **2** (Fig. 3). Resonance structures predict carbene carbon stabilization of C5- and C2-monocarbene complexes to reflect in the downfield shift of the H4 and H5 resonance, respectively. This is confirmed by experimental data, as

these resonances are the most downfield (Table 1). The favoured formation of **1** is due to the carbene fragment attaching to the least steric congested C5-position; representing a linear (open) arranged molecule, with stabilizing intra-ring electron delocalization between C5 (C_{carb}-acceptor) and C2-SBu (S-donor), Fig. 3(a). In contrast the main delocalization pathway between the C2′-SBu substituent and the C2-carbene substituent (*inside* to *inside*) is between the two thiophene rings in **2**, Fig. 3(b). Therefore ring, SBu and OEt proton resonances for **1** are significantly more downfield compared to **2**, indicating more stabilization/electron density delocalization towards the carbene carbon. Compared to C5- and C2-3,3′-BT monocarbene complexes, **1** and **2** respectively show no significant difference in proton resonances caused by the additional C2-SBu and C2′-SBu fragment, respectively [22].

Two classes of 3,3′-BT-2-SBu biscarbene complexes (**3** (C5,C2′-) and **4** (C5,C5′-)) were isolated from method 1 (Scheme 1), with **3** as the major product. Compared to the analogous Fischer carbene reaction with 3,3′-BT, the C5,C2′-biscarbene complex formed only in trace amounts and the major product was the C5,C5′-biscarbene complex (**9**) [22]. This leads to the supposition that the SBu fragment stabilizes the two carbene carbons in **3** through intra- and inter-ring electron delocalization, although sterically more crowded, where only intra-ring electron delocalization is possible in **4**. Again no significant difference in proton resonances caused by the additional SBu fragment is seen when comparing **4** with **9** (Table 1) [22].

The targeted [2,3-*b*;3′,2′-*d*]-DTT monocarbene compounds **10** (Cr) and **11** (W) have the proton resonance of the thienyl position adjacent to the carbene carbon (H4) most affected and shifted significantly downfield due to the strong electron-withdrawing properties of the metalcarbonyl-carbene moiety (Fig. 4). The H4 chemical shifts of **10** (8.47 ppm) and **11** (8.38 ppm) are slightly more downfield but comparable to their chromium (8.41 ppm) and tungsten (8.34 ppm) [2,3-*b*]-TT (thieno[2,3-*b*]thiophene) analogues respectively [21]. The methylene and methyl resonances are characteristic of chromium and tungsten ethoxycarbene fragments and exactly the same as their respective [2,3-*b*]-TT analogues [21].

The ^{1}H NMR spectrum of **7** is contaminated with **6** (Fig. 4). Compound **6** is known and the chemical shifts for the protons in the NEt fragment are found at 3.63 ppm (methylene group) and 1.44 ppm (methyl group) [20]. Replacing a carbonyl group with a CNEt ligand (**10** vs. **7**), which have very similar electronic bonding properties, has very little effect on the proton resonances. Protons H4′ and H5′ of **7** now resonate at 7.45 ppm as a broadened singlet and no longer appear as separate doublets at 7.47 and 7.50 ppm as for **10** (Fig. 4). The targeted [2,3-*b*;3′,2′-*d*]-DTT biscarbene complex (**5**) display H4 and ethoxy chemical shifts slightly but not significantly more downfield compared to its monocarbene analogue, **10**.

Replacing an ethoxy with a stronger π-donor amino substituent has a significant effect on H4, shifting the resonance upfield from 8.38 (**11**) to 6.86 ppm (**12**), due to the superior stabilization of Fischer carbene complexes by N-donor heteroatoms compared to oxygen. This results in a marked quenching of the electron withdrawing effect of the carbene metal carbonyl moiety, whereby the DTT-carbene substituent chemical resonances are not significantly shifted downfield from the precursor [2,3-*b*;3′,2′-*d*]-DTT chemical resonances (δ 7.40 ppm and 7.38 ppm). Manifestation of the bonding properties for the two methyl substituents (NMe_2) of **12** and **13** is found in two separate resonances, respectively, indicating that the methyl substituents are in different electronic environments due to restricted rotation around the C_{carb}–N bond.

2.2.2. ^{13}C NMR spectroscopy

The ^{13}C NMR data of the carbene complexes, recorded in $CDCl_3$, are summarized in Table 2. The electrophilic carbene carbon lacks electron density; hence its chemical shift appears in the most

Table 2
^{13}C NMR chemical shifts (δ) of the carbene complexes.

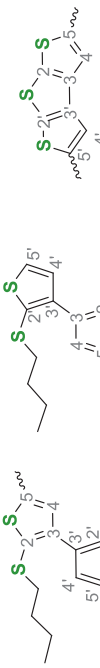

1, 3, 4

2

7, 10-13

Com-plex	C2	C3	C4	C5	C2′	C3′	C4′	C5′	SBu[a]	C_{carb}	C_{co} [c]	OEt[d]	NEt/NMe_2[e]
1	149.1	135.8	143.0	150.4	123.2	134.9	125.8	127.4	35.9, 30.6, 21.9, 13.5	307.6	223.1, 217.3	75.5, 15.3	
2	155.5	130.6	131.1	134.1	141.4	128.8	129.3	126.9	37.8, 31.1, 21.4, 13.5	323.8	223.1, 216.6	76.5, 14.0	
3	149.8	137.6	142.4	150.6	155.6	129.0	130.6	135.2	35.5, 30.6, 21.8, 13.4	C5: 307.5 C2′: 322.7	C5: 223.0, 217.3 C2′: 223.0, 216.5	C5: 75.6, 15.2 C2′: 76.6, 14.1	
4	149.1	136.7	142.4	150.9	131.7	134.6	140.6	155.1	36.2, 31.6, 22.6, 13.5	C5: 308.7 C5′: 316.6	C5: 223.1, 217.2 C5′: 223.2, 216.8	C5: 75.6, 14.1 C5′: 76.1, 15.1	
7	[f]	[f]	131.4	157.0	[f]	[f]	118.9	128.4		316.6, 167.5[b]	228.9, 223.0, 220.1	74.6, 15.5	39.4, 15.3
10	150.7	[f]	132.6	156.8	[f]	[f]	119.1	128.8		312.3	223.1, 217.1	75.9, 15.2	
11	151.5	[f]	133.2	159.8	[f]	[f]	119.1	128.8		286.9	202.3, 197.6	78.3, 14.9	
12	[f]	[f]	110.5	155.7	[f]	[f]	118.8	128.0		249.6	203.7, 198.2		53.9, 45.5
13	[f]	[f]	110.3	155.9						249.3	203.6, 198.1		54.0, 45.7

[a] Carbon chemical shifts for the $SCH_2CH_2CH_2CH_3$ fragment are reported with the first value being the chemical shift of the first methylene group after the sulpher atom, followed by the second and third methylene group's values. The last chemical shift belongs to the methyl group.
[b] Chemical shift belonging to CNEt of **7**, is listed under the C_{carb} column.
[c] Carbon chemical shifts for the metalcarbonyls are reported with the first value being the chemical shift of the carbonyl *trans* to the carbene carbon, and the second the chemical shift of the carbonyls *cis* to the carbene carbon. In the case of **7**, two *trans* signals are reported first (one *trans* to the carbene carbon and one *trans* to CNEt) followed by one *cis* signal (*trans* to CO) that is higher in intensity.
[d] Carbon chemical shifts for the ethoxy fragment are reported with the first value being the chemical shift of the methylene group, and the second the chemical shift of the methyl group.
[e] Carbon chemical shifts for the NEt fragment (**7**) are reported with the first value being the chemical shift of the methylene group, and the second the chemical shift of the methyl group. In the case of **12** and **13** the chemical shifts represent the methyl groups of NMe_2.
[f] Assignments could not be made unambiguously.

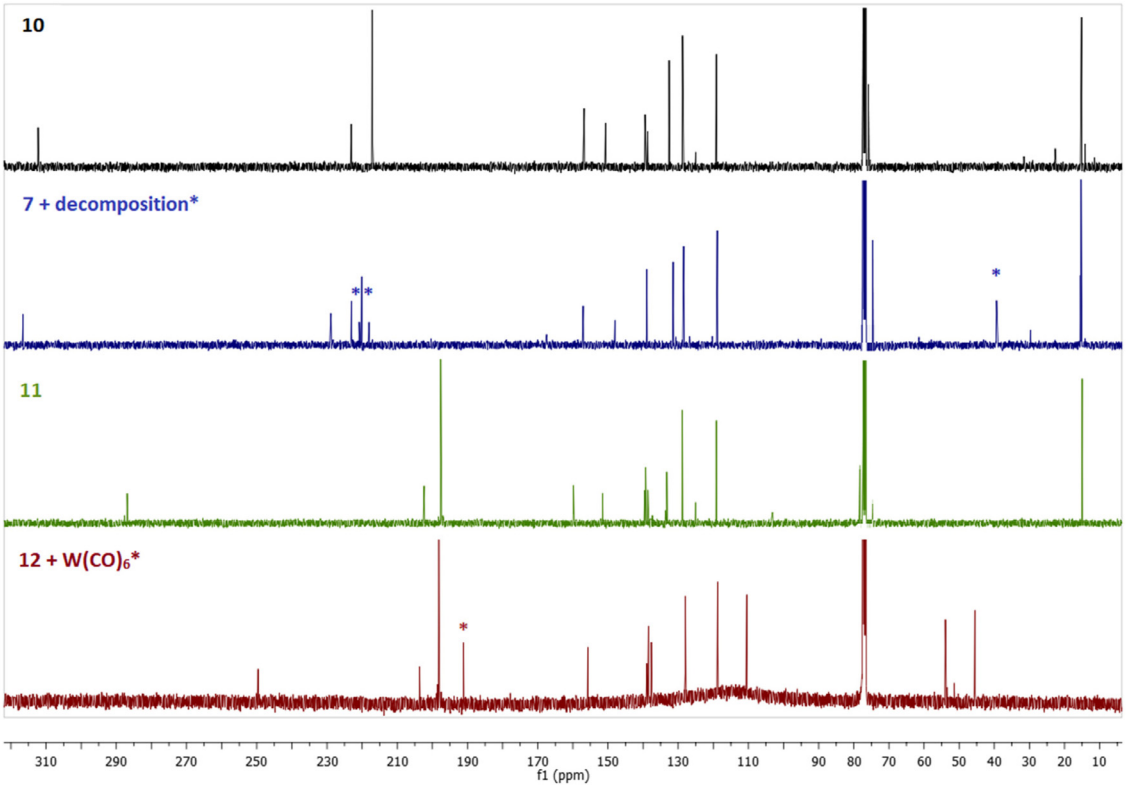

Fig. 5. ^{13}C NMR spectra showing chemical shift patterns for **7**, **10**–**12**.

downfield region of the ^{13}C NMR spectra. The carbene carbon chemical shifts are influenced by the nature of substituents and the positions where the carbene carbons are attached in the complexes. The carbene carbon of **2** (C2-carbene fragment) resonates *ca.* 15 ppm more downfield compared to **1** (C5-carbene fragment), Table 2. This is also the trend in analogous 3,3′-BT carbene complexes (330.1 and 316.3 ppm, respectively) [22]. The carbene carbon chemical shifts of 3,3′-BT C2- and C5-monocarbene complexes are at *ca.* 7 ppm lower field compared to their analogous 3,3′-BT-2′/2-SBu carbene complexes, **2** and **1** resepctively [22]. In the case of **4**, the carbene carbon resonance of its C5′-carbene fragment (on the C3′-ring without a C2-SBu fragment) is *ca.* 4 ppm more downfield compared to the carbene carbon signal of its C5-carbene fragment (on the C3-ring containing C2-SBu). This we ascribe to the donating property of the SBu-substituent into the carbene carrying thiophene ring, once connected *via* a conjugated pathway with a strong withdrawing carbene carbon on the same thiophene ring (Fig. 3). The carbene carbon signal of the C5′-carbene fragment of **4** (155.1 ppm, Table 2) is similar to the carbene carbon resonance of **9** (155.8 ppm), the analogous 3,3′-BT biscarbene complex [22].

The observation of π-donation is in contrast with the σ-inductive electron withdrawing effect of the SBu-fragment on the thienyl substituent. This is a consequence of replacing H by a more electronegative S atom. In **1** and **2**, the presence of the SBu-group results in a *ca.* 20 ppm downfield shift of C2 and C2′ respectively, when compared to their 3,3′-BT equivalents (129.1 (C2) and 122.4 ppm (C2′), respectively) [22]. The same principle is seen when comparing the C3-ring (containing a SBu fragment) of **4** with its own C3′-ring (without a SBu fragment) and again with **9** (SBu fragment is absent). Hence carbene complexes with 3,3′-BT-2/2′-SBu substituents have less electron density in the thienylene substituent to stabilize the carbene carbons compared to 3,3′-BT carbene complexes.

In the ^{1}H NMR spectrum of **7**, the presence of **6** can be observed. However, because of the long data acquisition time needed to acquire the ^{13}C NMR spectrum of **7**, decomposition of **6** is observed, accompanied with the absence of signals belonging to **6** (Fig. 5) [20]. When one carbonyl group of **10** is replaced with CNEt to give **7**, downfield shifts are seen in the carbene carbon and the carbonyl groups' resonances (Fig. 5). The carbonyl signals change from a characteristic pentacarbonyl fingerprint (one *trans* and one *cis*) to a tetracarbonyl fingerprint (two *trans* and one *cis*).

Characteristic values for different transition metals are seen in the resonances of carbene carbons and carbonyl groups. These resonances are *ca.* 23 ppm downfield when comparing **10** (Cr) with **11** (W) (Fig. 5), and similar to their respective analogous [2,3-*b*]-TT carbene complexes [21]. The aromatic carbon most affected by a carbene fragment is the carbon *ipso* to the carbene carbon. Comparing C3′-ring resonances of **3** and **4**, the *ipso* carbons (C2′ and C5′ respectively) are *ca.* 20 ppm downfield compared to their carbene free analogue C2′ and C5′ positions in **4** and **3** respectively, Table 2. The chemical shifts for the carbene carbon atom and C4 of aminocarbene complex **12** is lowered by *ca.* 37 and 23 ppm, respectively, compared to ethoxycarbene complex **11**, with the same metal and thienylene substituent. The two methyl substituents of NMe_2 in **12** and **13** resonate as separate peaks in their ^{13}C NMR spectra, *ca.* 8 ppm apart. Due to the reactivity of **5**, no ^{13}C NMR spectrum could be obtained for this compound, as decomposition occurred during the long data acquisition time needed to observe the carbene carbon resonance.

2.2.3. FT-IR spectroscopy

All the compounds represent a $M(CO)_5L$ system [24], with the exception of **7**, and their IR data are summarized in Table 3. Compound **4** was isolated in trace amounts as an inseparable mixture along with **3** and due to their similar chemical properties, they could not be purified further. The $A_1^{(2)}$ and E bands of **5**, **12** and **13** overlap to give one strong broad band in each case (Table 3).

The *cis*-$M(CO)_4L_2$ system (**7**) has C_s symmetry and display four IR and Raman active carbonyl stretching frequency modes ($2A_1$, B_1

Table 3
FT-IR data of complexes measured in hexane.

Compound	ν_{CO}, cm^{-1} $A_1^{(1)}$ (*m*)	B_1 (*vw*)	$A_1^{(2)}$ (*sh*)	E (*vs*)	B_2 (*s*)	ν_{CN}, cm^{-1} C≡N (*w*)
1	2056	1980	1952	1944		
2	2059	1985	1956	1947		
3	2056	1986	1955	1947		
5[a]	2059	1986	1943 (*vs*)	1943		
6[20]	2067	n.o.	1961	1961		2167
7	2015	1929 (*s*)	1941 (*m*)		1923	2162, 2129
10	2058	1983	1957	1947		
11	2066	1982	1952	1944		
12	2063 (*w*)	1974	1930 (*s*)	1930 (*s*)		
13	2063 (*w*)	1973	1936 (*s*)	1936 (*s*)		

[a]Sample measured in DCM, as ester formation occurred due to the compound's reactivity (C=O stretching band at 1710 cm^{-1}).

Table 4
Selected bond lengths (Å) and angles (°) of **1**, **5**, **7** and **10**–**13**.

Complex Bond lengths	1	5[c]	7	10	11	12	13[c]
M−C_{carb}	2.082(3)	2.075(3), 2.070(3)	2.063(2)	2.051(2)	2.200(6)	2.232(8)	2.21(1) , 2.24(1)
C_{carb}−OEt/NMe_2	1.336(3)	1.323(4), 1.326(3)	1.331(3)	1.332(3)	1.341(8)	1.31(1)	1.34(2) , 1.28(2)
M−CO *trans to CO*[a]	1.901(2)	1.900(3), 1.900(3)	1.897(2)	1.896(3)	2.039(8)	2.039(9)	2.04(2) , 2.03(2)
M−CO *trans to Ccarb*	1.870(4)	1.863(3), 1.881(3)	1.860(2)	1.879(3)	2.022(8)	2.00(1)	2.04(2) , 2.01(2)
M−CO *trans to CNEt*			1.875(2)				
M−CNEt			1.996(2)				
C_{carb}−C5	1.444(3)	1.457(3), 1.448(4)	1.459(2)	1.462(3)	1.450(9)	1.50(1)	1.50(1), 1.52(1)
C2−C3	1.396(4)	1.385(4), 1.381(3)	1.389(3)	1.388(3)	1.37(1)	1.39(1)	1.40(2), 1.39(2)
C3−C4	1.405(3)	1.406(3), 1.405(4)	1.412(2)	1.411(3)	1.409(9)	1.43(1)	1.44(2), 1.44(2)
C4−C5	1.385(3)	1.367(4), 1.372(3)	1.376(3)	1.379(3)	1.39(1)	1.36(1)	1.34(2), 1.35(1)
S−C2	1.712(2)	1.711(2), 1.701(2)	1.704(2)	1.706(2)	1.704(8)	1.72(1)	1.70(2), 1.73(1)
S−C5	1.744(3)	1.767(3), 1.764(3)	1.766(2)	1.766(2)	1.757(6)	1.750(9)	1.76(1), 1.76(1)
Bond angles							
M−C_{carb}−O/N	129.0(2)	130.5(2), 129.2(2)	129.5(1)	128.4(2)	128.5(5)	131.1(6)	130.9(9), 131.8(9)
M−C_{carb}−C5	126.0(2)	123.4(2), 125.1(2)	125.5(1)	126.2(1)	126.2(5)	116.4(5)	117.2(8), 114.1(8)
O/N−C_{carb}−C5	105.0(2)	106.1(2), 105.6(2)	105.0(2)	105.4(2)	105.3(5)	112.5(7)	112(1), 114(1)
Torsion angles							
M−C_{carb}−C5−C4	-2.9(4)	-6.5(4), 12.7(4)	-0.3(3)	2.0(3)	-4(1)	88(1)	80(1), -80(1)
O/N−C_{carb}−C5−C4	176.8(3)	175.5(2), -170.1(2)	180.0(2)	-178.1(2)	177.5(7)	-91(1)	-100(2), 104(2)
Angle between two mean planes[b]	2.38	7.39, 8.87	0.79	1.65	3.61	88.75	81.52, 79.86

[a]Averaged bond length.
[b]First mean plane drawn through C2, C3, C4 and C5, and the second through M, C_{carb} and O/N.
[c]First set reported for M1 and the second for M2.

and B_2). Two C≡N stretching vibrational bands are observed for **7** (containing a CNEt ligand). These bands represent symmetric vibrations and loss of degeneracy due to asymmetry of the system. C–N, C–C and C–O vibrations are observed in the same absorption region (1300–800 cm^{-1}) and the same counts for the C=N, C=C and C=O vibrations (1900–1500 cm^{-1}) [25] . Therefore C–N stretching vibrations of **7, 12** and **13** cannot be assigned unambiguously.

2.3. Molecular structures

The carbene complexes were crystallized by dissolving samples in DCM, layering the saturated solution with hexane, and allowing the crystals to form at low temperatures by slow diffusion and evaporation.

Single crystal X-ray diffraction studies confirmed the molecular structures of complexes **1**, **5**, **7** and **10**–**13** (Fig. 6). Selected bond lengths, angles and torsion angles are given in Table 4, employing the atom numbering scheme used in the NMR assignments. Crystal structures of ethoxy- and amino-[2,3-*b*;3′,2′-*d*]-DTT carbene complexes have similar features. In each case the planar [2,3-*b*;3′,2′-*d*]-DTT spacer has an ethoxy/amino substituent appearing on the same side as its sulphur atoms, along with an octahedral metal pentacarbonyl fragment attached to the spacer through an ethoxy/aminocarbene carbon. Carbene complexes have an electronic and steric favoured orientation, the *Z*-isomer, where the ethyl group and metal moiety are on the same side of the $((CO)_5M)C_{carb}$−O(Et) bond in the solid state [26–28]. All the ethoxycarbene complexes reported have the preferred *Z*-isomer arrangement, where the stereoelectronic interaction of the alkyl substituent and a *cis*-CO ligand prevails against the steric repulsion in alkoxy Fischer carbene complexes [29].

To determine if the thienylene spacer, carbene carbon, metal and ethoxy/amino fragment are all in the same plane, for each structure a mean plane was drawn through C2, C3, C4 and C5, and a second through M, C_{carb} and O/N. The angle between the two planes was measured, revealing that most of the crystal structures have a planar arrangement. Steric congestion in **5** prevents the molecule from being planar and the angles between the two mean planes, on each side of the molecule, are 7.39 and 8.87°. These angles are significantly greater in **12** and **13** (Table 4), due to the rigid, curved and condensed DTT backbone and the bulky dimethylamine fragment/s resulting in a more crowded molecule. This result is supported by the torsion angles M−C_{carb}−C5−C4 and O/N−C_{carb}−C5−C4 reported in Table 4.

The M−C_{carb} bond lengths for the chromium ethoxycarbene complexes range from 2.051(2) to 2.082(3) Å. Compounds **10** (2.051(2) Å), and **5** (2.075(3) and 2.070(3) Å) have M−C_{carb} bond lengths that are significantly different compared to their chromium mono- and bis-[2,3-*b*]-TT carbene analogue complexes (2.083(5)

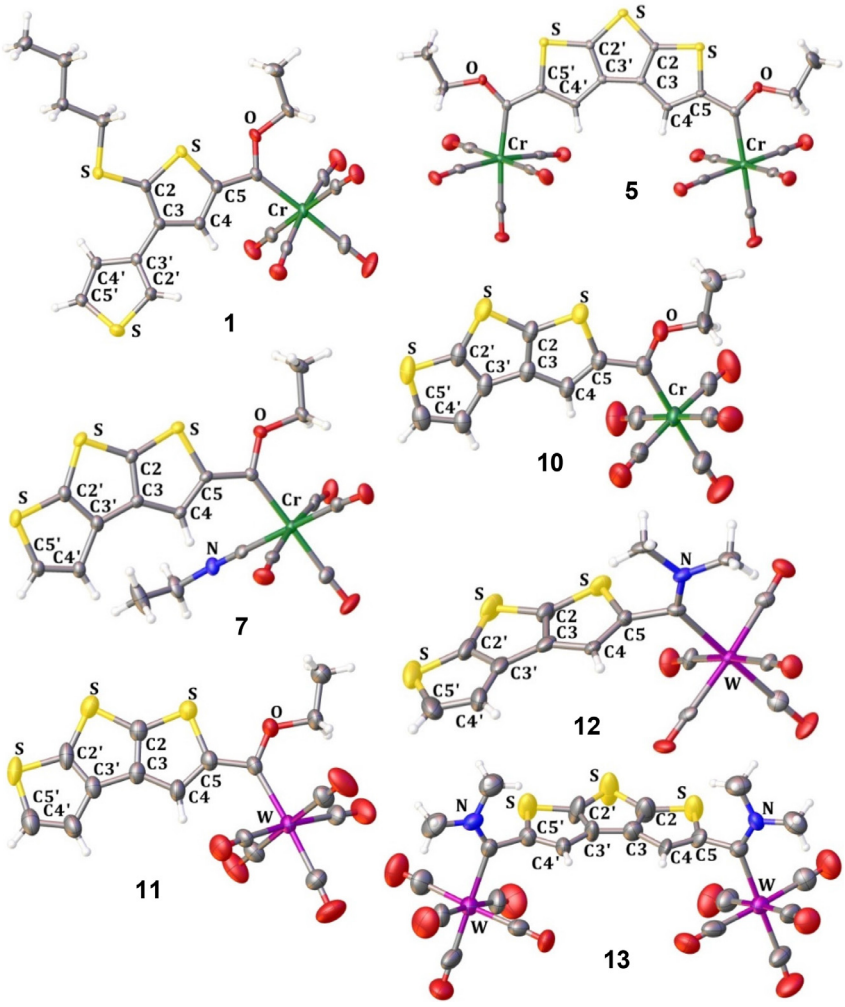

Fig. 6. The molecular structures of **1**, **5**, **7** and **10**–**13** with the atomic displacement ellipsoids shown at the 50% probability level.

and 2.058(4) Å), respectively [30]. The M–C_{carb} bond distance is significantly shorter in the ethoxycarbene complex **11** compared with the analogous aminocarbene complex **12**, emphasizing a smaller demand on π-interaction from the $W(CO)_5$ substituent in **12** because of the amino substituent's greater contribution.

From inspection of the C_{carb}–C5 bond lengths, it is evident that **12** and **13** (aminocarbene complexes) are less dependent on electron density from the thienylene substituent to stabilize the carbene carbon compared to the crystal structures of the ethoxycarbene complexes, hence their significantly longer bond lengths, as expected from the conclusions drawn from the NMR data. The M–CO $_{trans\ to\ Ccarb}$ bond lengths of the compounds are shorter than the M–CO $_{trans\ to\ CO}$ bond lengths and the respective averaged M–CO bond length of $Cr(CO)_6$ and $W(CO)_6$ [31,32]. This is a result of poorer π-acceptor properties of the carbene carbon compared to a carbonyl ligand and the *trans to* C_{carb} carbonyl ligand compensates for this by increasing metal-to-carbonyl-carbon backbonding. The same principle in seen in **7**, where the longer M–CNEt bond length is compensated for by the shorter M–CO bond length *trans to CNEt* (Table 4). This places the CNEt ligand as intermediate between a carbene and a carbonyl ligand based on bonding interactions.

The representative angles around the carbene carbon of *ca.* 130° (M–C_{carb}–O), 125° (M–C_{carb}–C5) and 105° (O–C_{carb}–C5) are observed for the ethoxycarbene complexes (Table 4 and Figure 6). In the case of aminocarbene complexes (**12** and **13**) the M–C_{carb}–C5 bond angles are significantly decreased and the N–C_{carb}–C5 bond angles increased as a result of the sterically crowded carbene substituents (Figure 7). The aminocarbene substituent, because of electronic involvement with the carbene carbon, places the methyl groups of the nitrogen in unfavourable planar orientations with respect to the bulky metal carbonyl fragment. The thiophene substituent rotates out of the plane to alleviate congestion. As a result, the DTT substituent now has an unfavourable orientation of the ring pi-cloud to effectively overlap with the carbene p_π-orbital.

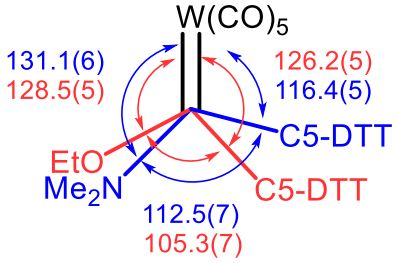

Fig. 7. Bond angles (°) around the carbene carbon of 11 (red) and 12 (blue). (For interpretation of the references to colour in this figure legend, the reader is referred to the web version of this article.)

Cis carbonyl ligands in the equatorial plane are staggered equally relative to the carbene ligand. Two carbonyl ligands *trans* to each other are slightly bent away from the carbene carbon in

the case of **1** (6.7(1)°), **5** (8.5(1)°), **7** (6.8(1)°), **11** (6.1(3)°), **12** (four carbonyls: 5.1(4) and 6.6(3)°) and **13** (5.4(7)°) as is seen from their CO-Cr/W-CO angles.

The two thiophene rings in **1** are non-planar as indicated by the inter-ring torsion angles C2−C3−C3′−C2′ of 145.3(2)° and C4−C3−C3′−C4′ of 146.4(2)°, striking a balance between electronic and steric factors. Little inter-ring conjugation/electron delocalization between the thiophene rings occur, as concluded from the ^{1}H NMR spectral data. Rotation around the inter-ring bond of the thiophene rings generates two positions for the sulphur atom of the second thiophene ring. Two molecules are observed in the unit cell; one molecule with the sulphur atom of the second thiophene ring rotated to the same side as the first sulphur atom in the spacer and in the second molecule the second thiophene ring is rotated away from the other sulphur atom in the spacer. The one molecule showed distortion of the SBu fragment. Compounds **10** and **11** packed in a similar fashion, with π-π interaction distances measured at 3.250 and 3.940 Å, respectively (Fig. S6, Supplementary data), while the solid state structure of **13** packs such that both stacking and columnar packing is observed when viewed down two different axes (Fig. S7, Supplementary data).

3. Conclusions

The use of a more reactive isomer [2,3-*b*;3′,2′-*d*]-DTT, as an annulated thiophene substrate for the preparation of Fischer carbene complexes with different bases, revealed unexpected ring-opened products. The central sulphur atom of [2,3-*b*;3′,2′-*d*]-DTT was attacked by organolithium reagents (*e.g.* *n*-BuLi) or amine nucleophiles (HDA). While using *n*-BuLi the majority of carbene complexes formed resulted from a ring-opened DTT spacer. Nucleophilic attack on the central thiophene sulphur by *n*-BuLi afforded a SBu substituent on the inside position of a 3,3′-BT-2-SBu backbone. Employment of nucleophilic HDA/*n*-BuLi again resulted in attack by HDA on the central sulphur atom, but this time with excision of the central sulphur atom, producing mono- and biscarbene complexes of 3,3′-BT. In both instances carbene complexes from deprotonated DTT were spectroscopically observed, but could not be isolated. Although deprotonation was observed, KHMDS also facilitated unprecedented nucleophilic addition to the carbonyl carbon atom of chromium hexacarbonyl to afford K[Cr(CO)$_5${CN}].

To circumvent the ring-opening reactions, the α-positions of [2,3-*b*;3′,2′-*d*]-DTT were first activated to produce 5,5′-dibromo-[2,3-*b*;3′,2′-*d*]-DTT, prior to carrying out preparative Fischer carbene reactions. Ethoxy-monocarbene complexes of [2,3-*b*;3′,2′-*d*]-DTT were isolated by using this method, but biscarbene complexes formed either in very low yield (Cr) or could not be isolated (W) as a result of the greater reactivity of [2,3-*b*;3′,2′-*d*]-DTT complexes, compared to their [3,2-*b*;2′,3′-*d*]-DTT analogues [12–15]. This is presumably due to the greater extent of π-conjugation. To isolate the [2,3-*b*;3′,2′-*d*]-DTT biscarbene tungsten complex, the reaction mixture obtained from the Fischer carbene reaction starting with 5,5′-dibromo-[2,3-*b*;3′,2′-*d*]-DTT, was first aminolysed before purification. Aminolysis of ethoxycarbene complexes is known to improve the stability of the carbene complexes by having a more electron donating amino group, stabilizing the electrophilic carbene carbon.

4. Experimental

4.1. Methods and materials

All operations were carried out using standard Schlenk techniques or vacuum line techniques under an inert atmosphere of nitrogen or argon, using oven-dried glassware. Silica gel 60 (particle size 0.063–0.20 mm) was used as resin (stationary phase) for all column chromatography separations.

Triethyloxonium tetrafluoroborate was prepared according to literature procedure and stored in diethyl ether under Ar (g) [33]. Boron trifluoride etherate was distilled before use. Under N_2 atmosphere THF and diethyl ether were distilled over sodium wire and benzophenone, hexane and benzene over sodium wire and DCM and acetonitrile over CaH_2. $CDCl_3$ was dried over CaH_2. Other chemicals commercially supplied by Sigma Aldrich and Strem Chemicals were used as received. The *n*-BuLi used in syntheses, was from a stock 1.6 M solution in hexane.

P1 was prepared from 3-bromothiophene that involved coupling of two thiophene rings using a lithium bromide exchange and copper chloride mediated coupling, followed by bromination with N-bromosuccinimide (NBS). Another lithium bromide exchange and thio-ring closure with S(PhSO$_2$)$_2$ yields pure **P1** after standard reaction work-up and purification [3,16]. **P2** is prepared by bromination of **P1** with NBS.[3] Assignment of the NMR resonances of these precursors is given in the Supplementary data (Fig. S1).

Compounds **1**, **2**, **7** and **10** could not be characterized using mass spectrometric (MS) analysis as the compounds did not ionize during the technique. In the case of **4**, only NMR analysis was carried out as the compound was obtained as an inseparable mixture along with **3**. The low yield of **5** resulted in too small a sample size to collect ^{13}C NMR or MS data.

4.1.1. NMR spectroscopy

NMR spectra were recorded on Ultrashield Plus 400 AVANCE 3 and Ultrashield 300 AVANCE 3 spectrometers, at 25 °C. The ^{1}H NMR spectra were recorded at 400.13 or 300.13 MHz, and the ^{13}C NMR spectra at 100.613 or 75.468 MHz, respectively. The samples were measured in solvent $CDCl_3$, chemical shifts (reported as δ (ppm) downfield from Me_4Si) are referenced at 7.26 ppm for δ_H and 77.0 ppm for δ_C. Coupling constants (J) are reported in Hz. Preparation of the samples was carried out under Ar (g) and the NMR tubes were sealed before data collection. The ^{1}H NMR data are reported in the format: chemical shift (integration, multiplicity, coupling constant, assignment) and the ^{13}C NMR data in the format: chemical shift (assignment), in the order of assignments. The spectral coupling patterns are: s – singlet, d – doublet, t – triplet, q – quartet and m – multiplet. First-order analysis is carried out to assign signals of the ^{1}H NMR spectra. Additional 2D [^{1}H, ^{1}H] COSY NMR experiments were done where confirmation of the proton assignments were required. Assigning the carbon chemical shifts, obtained from proton-decoupled ^{13}C NMR spectra, was possible with the assistance of 2D [^{1}H, ^{13}C] HSQC and 2D [^{1}H, ^{13}C] HMBC NMR experiments. Standard Bruker pulse programs were used in the experiments.

4.1.2. FT-IR spectroscopy

Infrared spectroscopy was performed on a Bruker ALPHA FT-IR spectrophotometer with a NaCl cell, using dried hexane as solvent. Insoluble samples were measured using dried DCM as solvent. The absorptions were measured from 400 to 4000 cm^{-1}. The IR data are reported in the format: absorption intensity (assignment) in the order of highest to lowest wavenumber. The wave intensities are: *vw* – very weak, *w* – weak, *m* – medium, *s* –strong, *vs* – very strong and *sh* – shoulder.

4.1.3. High resolution mass spectrometry

Mass spectral analyses were performed on a Waters® Synapt G2 high definition mass spectrometer (HDMS) that consists of a Waters Acquity Ultra Performance Liquid Chromatography (UPLC®) system hyphenated to a quadrupole-time-of-flight (QTOF) instrument. Data acquisition and processing was carried out with Mass-

LynxTM (version 4.1) software. A leucine encephalin solution (2 pg/μL, *m/z* 555.2693) was used as an internal lock mass control standard to compensate for instrumental drift and ensure good mass accuracy. The internal control was directly infused into the source through a secondary orthogonal electrospray ionization (ESI) probe to allowing intermittent sampling. Flow injection analysis (FIA, 0.4 mL/min flow rate) with the injection volume set at 5 µL. Samples were made up in ultra purity liquid chromatography methanol to an approximate concentration of 10 µg/mL. The methanol was spiked with 0.1% formic acid and used throughout the 1 min run. The capillary voltage for the ESI source was set at 2.6 kV for negative mode ionization. The source temperature was set at 110 °C, the sampling cone voltage at 25 V, extraction cone voltage at 4.0 V and cone gas (nitrogen) flow at 10.0 L/Hr. The desolvation temperature was set at 300 °C with a gas (nitrogen) flow of 600.0 L/Hr. The mass to charge ratios (*m/z*) were measured in the range of 50–1500 Da with the raw data presented in the form of a centroid profile (scans were collected every 0.3 s). Negative electron spray was chosen as the ionization technique. The MS data are reported in the format: calculated mass, found mass (percentage intensity, fragmentation) in the order of highest to lowest mass to charge ratio.

4.1.4. Single crystal X-ray diffraction

Single crystal diffraction data for **1, 5, 7, 10** and **13** were collected at 150 K on a Bruker D8 Venture diffractometer with a kappa geometry goniometer and a Photon 100 CMOS detector using a Mo-Kα IμS micro focus source. Data were reduced and scaled using SAINT and absorption intensity corrections were performed using SADABS (APEX III control software) [34]. Single crystals of **11** and **12** were analysed on a Rigaku XtaLAB Synergy R diffractometer, with a rotating-anode X-ray source and a HyPix CCD detector. Data reduction and absorption were carried out using the CrysAlisPro (version 1.171.40.23a) software package [35]. X-ray diffraction measurements were performed at 150 K, using an Oxford Cryogenics Cryostat. All structures were solved by an intrinsic phasing algorithm using SHELXTS [36] and were refined by full-matrix least-squares methods based on F^2 using SHELXL [37]. All non-hydrogen atoms were refined anisotropically. All hydrogen atoms were placed in idealized positions and refined using riding models.

4.1.5. UV–Vis spectroscopy

Measurements were performed on 10 mL DCM solutions of 0.01 mM analyte concentration at 25 °C. Absorptions were measured in the range 200–1000 nm using a UV–Vis spectrophotometer Specord 200 plus. WinASPECT PLUS (version 4.2) software was used for data visualization.

4.1.6. Synthesis of complexes

Method 1: Lithiation of [2,3-*b*;3′,2′-*d*]-DTT using *n*-BuLi

n-BuLi (1.6 M in hexane, 2.1 mL, 3.3 mmol) was added to [2,3-*b*;3′,2′-*d*]-DTT (**P1**) (0.36 g, 1.8 mmol) dissolved in 20 mL of THF at −78 °C. After 30 min, $Cr(CO)_6$ (0.59 g, 2.7 mmol) was added to the reaction mixture. The solution stirred for 15 min at −78 °C, followed by 40 min at room temperature. The solvent was reduced *in vacuo*. The residue was dissolved in 10 mL DCM and cooled to −30 °C before being treated with $[Et_3O][BF_4]$ in DCM (1.33 g, 7.0 mmol). The reaction mixture was allowed to reach room temperature after which the solvent was reduced *in vacuo*. The products were purified using column chromatography starting with eluent *n*-hexane and increasing the polarity with DCM. The products isolated, in sequence of elution, are listed in Table S1, Supplementary data.

Compound 1: UV–Vis $\lambda_{max}(CH_2Cl_2)$/nm 491 (ε/dm^3 mol^{-1} cm^{-1} 23,990), 387 (8460). **FT-IR** ν_{CO}(hexane)/cm^{-1} 2056 m ($A_1^{(1)}$), 1980*vw* (B_1), 1952*sh* ($A_1^{(2)}$), 1944 vs (E). **^{1}H NMR** δ^1H(300.13 MHz; $CDCl_3$; Me_4Si) 8.28 (1 H, s, H4), 7.42 (1 H, dd, $^3J_{5',4'}$ 4.9 and $^4J_{5',2'}$ 2.5, H5′), 7.40 (1 H, dd, $^3J_{4',5'}$ 4.9 and $^4J_{4',2'}$ 1.3, H4′), 7.58 (1 H, dd, $^4J_{2',5'}$ 2.5 and $^4J_{2',4'}$ 1.3, H2′), 5.13 (2 H, q, ^3J 7.0, CH_2), 1.67 (3 H, t, ^3J 7.0, CH_3), 3.08 (2 H, t, ^3J 7.3, $SCH_2CH_2CH_2CH_3$), 1.76 (2 H, dt, ^3J 7.3, $SCH_2CH_2CH_2CH_3$), 1.50 (2 H, m, $SCH_2CH_2CH_2CH_3$), 0.96 (3 H, t, ^3J 7.3, $SCH_2CH_2CH_2CH_3$). **^{13}C NMR** δ^{13}C(75.468 MHz; $CDCl_3$; Me_4Si) 307.6 (C_{carb}), 223.1 (CO_{trans}), 217.3 (CO_{cis}), 150.4 (C5), 143.0 (C4), 135.8 (C3), 149.1 (C2), 127.4 (C5′), 125.8 (C4′), 134.9 (C3′), 123.2 (C2′), 75.5 (CH_2), 15.3 (CH_3), 35.9 ($SCH_2CH_2CH_2CH_3$), 30.6 ($SCH_2CH_2CH_2CH_3$), 21.9 ($SCH_2CH_2CH_2CH_3$), 13.5 ($SCH_2CH_2CH_2CH_3$).

Compound 2: UV–Vis $\lambda_{max}(CH_2Cl_2)$/nm 452 (ε/dm^3 mol^{-1} cm^{-1} 1740). **FT-IR** ν_{CO}(hexane)/cm^{-1} 2059 m ($A_1^{(1)}$), 1985*vw* (B_1), 1956*sh* ($A_1^{(2)}$), 1947 vs (E). **^{1}H NMR** δ^1H(400.13 MHz; $CDCl_3$; Me_4Si) 7.72 (1 H, d, $^3J_{5,4}$ 5.0, H5), 7.04 (1 H, d, $^3J_{4,5}$ 5.0, H4), 7.30 (1 H, d, $^3J_{5',4'}$ 5.4, H5′), 6.84 (1 H, d, $^3J_{4',5'}$ 5.4, H4′), 4.84 (2 H, q, ^3J 7.0, CH_2), 1.07 (3 H, t, ^3J 7.0, CH_3), 2.58 (2 H, t, ^3J 7.3, $SCH_2CH_2CH_2CH_3$), 1.41 (2 H, dt, ^3J 7.3, $SCH_2CH_2CH_2CH_3$), 1.25 (2 H, m, $SCH_2CH_2CH_2CH_3$), 0.80 (3 H, t, ^3J 7.3, $SCH_2CH_2CH_2CH_3$). **^{13}C NMR** δ^{13}C(100.613 MHz; $CDCl_3$; Me_4Si) 323.8 (C_{carb}), 223.1 (CO_{trans}), 216.6 (CO_{cis}), 134.1 (C5), 131.1 (C4), 130.6 (C3), 155.5 (C2), 126.9 (C5′), 129.3 (C4′), 128.8 (C3′), 141.4 (C2′), 76.5 (CH_2), 14.0 (CH_3), 37.8 ($SCH_2CH_2CH_2CH_3$), 31.1 ($SCH_2CH_2CH_2CH_3$), 21.4 ($SCH_2CH_2CH_2CH_3$), 13.5 ($SCH_2CH_2CH_2CH_3$).

Compound 3: UV–Vis $\lambda_{max}(CH_2Cl_2)$/nm 484 (ε/dm^3 mol^{-1} cm^{-1} 32,780), 380 (13,690). **FT-IR** ν_{CO}(hexane)/cm^{-1} 2056 m ($A_1^{(1)}$), 1986*vw* (B_1), 1955*sh* ($A_1^{(2)}$), 1947 vs (E). **^{1}H NMR** δ^1H(400.13 MHz; $CDCl_3$; Me_4Si) 8.01 (1 H, s, H4), 7.79 (1 H, d, $^3J_{5',4'}$ 5.0, H5′), 6.99 (1 H, d, $^3J_{4','}$ 5.0, H4′), 5.15 (2 H, q, ^3J 7.1, C5CH_2), 4.91 (2 H, q, ^3J 7.0, C2′CH_2), 1.68 (3 H, t, ^3J 7.1, C5CH_3), 1.14 (3 H, t, ^3J 7.0, C2′CH_3), 2.97 (2 H, t, ^3J 7.4, $SCH_2CH_2CH_2CH_3$), 1.68 (2 H, m, $SCH_2CH_2CH_2CH_3$), 1.41 (2 H, dt, ^3J 7.4, $SCH_2CH_2CH_2CH_3$), 0.93 (3 H, t, ^3J 7.4, $SCH_2CH_2CH_2CH_3$). **^{13}C NMR** δ^{13}C(100.613 MHz; $CDCl_3$; Me_4Si) 307.5 (C5C_{carb}), 322.7 (C2′C_{carb}), 223.0 (CO_{trans}, C5 and C2′), 217.3 (C5CO_{cis}), 216.5 (C2′CO_{cis}), 150.6 (C5), 142.4 (C4), 137.6 (C3), 149.8 (C2), 135.2 (C5′), 130.6 (C4′), 129.0 (C3′), 155.6 (C2′), 75.6 (C5CH_2), 15.2 (C5CH_3), 76.6 (C2′CH_2), 14.1 (C2′CH_3), 35.5 ($SCH_2CH_2CH_2CH_3$), 30.6 ($SCH_2CH_2CH_2CH_3$), 21.8 ($SCH_2CH_2CH_2CH_3$), 13.4 ($SCH_2CH_2CH_2CH_3$). **ESI-MS** *m/z* ($C_{28}H_{22}O_{12}S_3Cr_2$, 750.65 g/mol) calculated: 748.9005, found: 748.9352 (6%, $[M\text{-}H]^-$), calculated: 720.9056, found: 720.8736 (9%, $[M-CO-H]^-$), calculated: 692.9107, found: 692.8768 (4%, $[M-2CO-H]^-$), calculated: 664.9158, found: 664.8814 (7%, $[M-3CO-H]^-$).

Compund 4: ^{1}H NMR δ^1H(400.13 MHz; $CDCl_3$; Me_4Si) 8.32 (1 H, s, H4), 8.58 (1 H, d, $^4J_{4',2'}$ 0.8, H4′), 7.90 (1 H, d, $^4J_{2',4'}$ 0.8, H2′), 5.16 (2 H, q, ^3J 7.2, C5CH_2), 1.67 (3 H, t, ^3J 7.2, C5CH_3), 5.24 (2 H, q, ^3J 7.0, C5′CH_2), 1.71 (3 H, t, ^3J 7.0, C5′CH_3), 3.12 (2 H, t, ^3J 7.3, $SCH_2CH_2CH_2CH_3$), 1.78 (2 H, dt, ^3J 7.3, $SCH_2CH_2CH_2CH_3$), 1.50 (2 H, m, $SCH_2CH_2CH_2CH_3$), 0.98 (3 H, t, ^3J 7.3, $SCH_2CH_2CH_2CH_3$). **^{13}C NMR** δ^{13}C(100.613 MHz; $CDCl_3$; Me_4Si) 308.7 (C5C_{carb}), 316.6 (C5′C_{carb}), 223.1 (C5CO_{trans}), 223.2 (C5′CO_{trans}), 217.2 (C5CO_{cis}), 216.8 (C5′CO_{cis}), 150.9 (C5), 142.4 (C4), 136.7 and 134.6 (C3 and C3′), 149.1 (C2), 155.1 (C5′), 140.6 (C4′), 131.7 (C2′), 75.6 (C5CH_2), 14.1 (C5CH_3), 76.1 (C5′CH_2), 15.1 (C5′CH_3), 36.2 ($SCH_2CH_2CH_2CH_3$), 31.6 ($SCH_2CH_2CH_2CH_3$), 22.6 ($SCH_2CH_2CH_2CH_3$), 13.5 ($SCH_2CH_2CH_2CH_3$).

Compound 5: UV–Vis $\lambda_{max}(CH_2Cl_2)$/nm 477 (ε/dm^3 mol^{-1} cm^{-1} 3360). **FT-IR** ν_{CO}(DCM)/cm^{-1} 2059 m ($A_1^{(1)}$), 1986*vw* (B_1), 1943 vs ($A_1^{(2)}$ and E), 1710 m (C=O stretching vibration). **^{1}H NMR** δ^1H(300.13 MHz; $CDCl_3$; Me_4Si) 8.49 (2 H, s, H4), 5.21 (4 H, q, ^3J 7.0, CH_2), 1.71 (6 H, t, ^3J 7.0, CH_3).

Method 2: Deprotonation of [2,3-*b*;3′,2′-*d*]-DTT using KHMDS

KHMDS (0.86 g, 4.3 mmol) was added to [2,3-*b*;3′,2′-*d*]-DTT (**P1**) (0.36 g, 1.8 mmol) and $Cr(CO)_6$ (0.79 g, 3.6 mmol) dissolved in

20 mL of THF at -78 °C. After 30 min at -78 °C the solution was allowed to reach room temperature for 1 hour. The solvents were reduced *in vacuo*. The residue was dissolved in 10 mL DCM and cooled to -30 °C, then treated with $[Et_3O][BF_4]$ in DCM (1.33 g, 7 mmol). The reaction mixture was allowed to reach room temperature after which the solvent was reduced *in vacuo*. Column chromatographic purification of the products was carried out using *n*-hexane and DCM as eluents. The products isolated, in sequence of elution, are listed in Table S2, Supplementary data.

Compound 6: ^{1}H NMR δ^1H(400.13 MHz; $CDCl_3$; Me_4Si) 3.63 (2 H, q, ^3J 7.0, CH_2), 1.44 (3 H, t, ^3J 7.0, CH_3). **^{13}C NMR** δ^{13}C(100.613 MHz; $CDCl_3$; Me_4Si) 217.2 (CO_{trans}), 214.9 (CO_{cis}), 160.4 (CNEt), 39.4 (CH_2), 15.1 (CH_3). The ^{13}C NMR assignment is based on literature reports for this known compound [21].

Compound 7: UV–Vis $\lambda_{max}(CH_2Cl_2)$/nm 506 (ε/dm^3 mol^{-1} cm^{-1} 5010). **FT-IR** ν(hexane)/cm^{-1} 2162 w and 2129 w (ν_{CN}), 2015 m ($A_1^{(1)}$), 1941 m ($A_1^{(2)}$), 1929s (B_1) and 1923s (B_2) (ν_{CO}). **^{1}H NMR** δ^1H(400.13 MHz; $CDCl_3$; Me_4Si) 8.43 (1 H, s, H4), 7.45 (2 H, s, H4′ and H5′), 5.21 (2 H, q, ^3J 6.9, CH_2), 1.64 (3 H, t, ^3J 6.9, CH_3), 3.57 (2 H, q, ^3J 7.2, N*C*H_2CH$_3$), 1.32 (3 H, t, ^3J 7.2, NCH$_2$*C*H_3). **^{13}C NMR** δ^{13}C(100.613 MHz; $CDCl_3$; Me_4Si) 316.6 (C_{carb}), 228.9 and 223.0 (CO_{trans}), 220.1 (CO_{cis}), 167.5 (CNEt, value compared to similar compounds),[39] 157.0 (C5), 131.4 (C4), 148.0, 139.0, n.o. and 138.9 (C3, C2, C3′ and C2′), 128.4 (C5′), 118.9 (C4′), 74.6 (CH_2), 15.5 (CH_3) 39.4 (N*C*H_2CH$_3$), 15.3 (NCH$_2$*C*H_3).

Method 3: Deprotonation of [2,3-*b*;3′,3′-*d*]-DTT using HDA and *n*-BuLi

To the reaction vessel was added diisopropylamine (0.53 mL, 3.8 mmol) in 10 mL THF at −78°C, followed by the addition of *n*-BuLi (1.6 M in hexane, 2.4 mL, 3.8 mmol). [2,3-*b*;3′,2′-*d*]-DTT (**P1**) (0.32 g, 1.6 mmol) was dissolved in 10 mL of THF at -78 °C and transferred to the HDA and *n*-BuLi mixture using a cannula. After 30 min at −78 °C, $Cr(CO)_6$ (0.70 g, 3.2 mmol) was added to the cream coloured solution and allowed to stir at this temperature before the yellow solution was allowed to reach room temperature for 1 hour, turning the colour red brown. The solvent was reduced *in vacuo*. The residue was dissolved in 10 mL DCM and cooled to −30 °C then treated with $[Et_3O][BF_4]$ in DCM (1.33 g, 7.0 mmol), resulting in a purple red solution. The reaction mixture was allowed to reach room temperature after which the solvent was reduced *in vacuo*. The products were purified using gradient column chromatography with solvents *n*-hexane and DCM. The products isolated, in sequence of elution, are listed in Table S3, Supplementary data.

Method 4: Debromination of 5,′-dibromo-[2,3-*b*;3′,′-*d*]-DTT using *n*-BuLi to synthesize chromium carbene complexes

5,5′-Dibromo-[2,3-*b*;3′,2′-*d*]-DTT (**P2**) (0.15 g, 0.43 mmol) was dissolved in 10 mL of THF at −78 °C. *n*-BuLi (0.63 mL, 1 mmol) was added, resulting in a yellow reaction mixture. After 30 min at −78 °C, $Cr(CO)_6$ (0.22 g, 1 mmol) was added to the solution and allowed to stir at this temperature before the orange solution was allowed to reach room temperature for 1 hour. The solvent was reduced *in vacuo*. The residue was dissolved in 10 mL DCM and cooled to −30 °C then treated with $[Et_3O][BF_4]$ in DCM (0.38 g, 2.0 mmol). The reaction mixture was allowed to reach room temperature, turning the colour red purple, after which the solvent was reduced *in vacuo*. The products were purified using column chromatography starting with *n*-hexane and increasing the polarity with DCM. The products isolated, in sequence of elution, are listed in Table S4, Supplementary data.

Compound 10: UV–Vis $\lambda_{max}(CH_2Cl_2)$/nm 481 (ε/dm^3 mol^{-1} cm^{-1} 14,450), 356 (11,000). **FT-IR** ν_{CO}(hexane)/cm^{-1} 2058 m ($A_1^{(1)}$), 1983*vw* (B_1), 1957*sh* ($A_1^{(2)}$), 1947 vs (E). **^{1}H NMR** δ^1H(400.13 MHz; $CDCl_3$; Me_4Si) 8.47 (1 H, s, H4), 7.47 (1 H, d, $^3J_{5',4'}$ 5.2, H5′), 7.50 (1 H, d, $^3J_{4',5'}$ 5.2, H4′), 5.18 (2 H, q, ^3J 7.0, CH_2), 1.69 (3 H, t, ^3J 7.0, CH_3). **^{13}C NMR** δ^{13}C(100.613 MHz; $CDCl_3$; Me_4Si) 312.3 (C_{carb}), 223.1 (CO_{trans}), 217.1 (CO_{cis}), 156.8 (C5), 132.6 (C4), 139.4, 138.7 and n.o. (C3, C3′ and C2′), 150.7 (C2), 128.8 (C5′), 119.1 (C4′), 75.9 (CH_2), 15.2 (CH_3).

Method 4: Debromination of 5,5′-dibromo-[2,3-*b*;3′,2′-*d*]-DTT using *n*-BuLi to synthesize tungsten carbene complexes

5,5′-Dibromo-[2,3-*b*;3′,2′-*d*]-DTT (**P2**) (1.06 g, 3 mmol) was dissolved in 50 mL of THF at −78 °C. *n*-BuLi (3.75 mL, 6 mmol) was added. After 10 min at −78 °C, $W(CO)_6$ (2.11 g, 6 mmol) was added to the solution and allowed to stir at this temperature for 1 hr before warming to room temperature. The solvent was reduced *in vacuo*. The residue was dissolved in 10 mL DCM and cooled to −30 °C then treated with $[Et_3O][BF_4]$ in DCM (2.28 g, 12 mmol). The reaction mixture was allowed to reach room temperature after which the solvent was reduced *in vacuo*. Column chromatographic purification of the products was carried out using *n*-hexane and DCM as eluents. The products isolated, in sequence of elution, are listed in Table S5, Supplementary data.

Compound 11: UV–Vis $\lambda_{max}(CH_2Cl_2)$/nm 469 (ε/dm^3 mol^{-1} cm^{-1} 21,850), 358 (12,290). **FT-IR** ν_{CO}(hexane)/cm^{-1} 2066 m ($A_1^{(1)}$), 1982*vw* (B_1), 1952*sh* ($A_1^{(2)}$), 1944 vs (E). **^{1}H NMR** δ^1H(400.13 MHz; $CDCl_3$; Me_4Si) 8.38 (1 H, s, H4), 7.47 (1 H, d, $^3J_{5',4'}$ 5.3, H5′), 7.49 (1 H, d, $^3J_{4',5'}$ 5.3, H4′), 5.00 (2 H, q, ^3J 7.1, CH_2), 1.67 (3 H, t, ^3J 7.1, CH_3). **^{13}C NMR** δ^{13}C(100.613 MHz; $CDCl_3$; Me_4Si) 286.9 (C_{carb}), 202.3 (CO_{trans}), 197.6 (CO_{cis}), 159.8 (C5),133.2 (C4), 139.6, 139.2 and 138.6 (C3, C3′ and C2′), 151.5 (C2), 128.8 (C5′), 119.1 (C4′), 78.3 (CH_2), 14.9 (CH_3). **ESI-MS** *m/z*($C_{16}H_8O_6S_3W$, 576.27 g/mol) calculated: 574.8914, found: 574.8440 (27%, $[M-H]^-$), calculated: 546.8965, found: 546.8470 (8%, $[M-H-CO]^-$), calculated: 518.9016, found: 518.9011 (21%, $[M-H-2CO]^-$).

Method 5: Synthesis of tungsten mono- and bisaminocarbene complexes of [2,3-*b*;3′,2′-*d*]-DTT

A mixture of tungsten mono- and bisethoxycarbene [2,3-*b*;3′,2′-*d*]-DTT complexes was dissolved in 10 mL THF. Dimethylamine hydrochloride (2.45 g, 30.0 mmol) and sodium hydroxide (1.20 g, 30.0 mmol) was added to the reaction mixture. Distilled H_2O was added dropwise until all the suspended salts were dissolved and a colour change was observed. The reaction was followed with TLC until all the starting material had reacted. THF was removed *in vacuo*, and the remaining residue extracted with ether. The ether layer was washed with a saturated solution of $NH(CH_3)_2$.HCl in distilled H_2O. The ether layer was dried over $MgSO_4$, filtered and the solvent was reduced *in vacuo*. The products were purified using gradient column chromatography with solvents *n*-hexane and DCM. The products isolated, in sequence of elution, are listed in Table S6, Supplementary data.

Compound 12: UV–Vis $\lambda_{max}(CH_2Cl_2)$/nm 350 (ε/dm^3 mol^{-1} cm^{-1} 6620). **FT-IR** ν_{CO}(hexane)/cm^{-1} 2063 w ($A_1^{(1)}$), 1974*vw* (B_1), 1930s (E and $A_1^{(2)}$). **^{1}H NMR** δ^1H(400.13 MHz; $CDCl_3$; Me_4Si) 6.86 (1 H, s, H4), 7.42 (1 H, d, $^3J_{5',4'}$ 5.2, H5′), 7.34 (1 H, d, $^3J_{4',}$ 5.2, H4′), 3.96 (3 H, s, CH_3), 3.33 (3 H, s, CH_3). **^{13}C NMR** δ^{13}C(100.613 MHz; $CDCl_3$; Me_4Si) 249.6 (C_{carb}), 203.7 (CO_{trans}), 198.2 (CO_{cis}), 155.7 (C5), 110.5 (C4), 138.9, 138.5, 137.7 and n.o. (C3, C2, C3′ and C2′), 128.0 (C5′), 118.8 (C4′), 53.9 and 45.5 (CH_3). **ESI-MS** *m/z*($C_{16}H_9NO_5S_3W$, 575.28 g/mol) calculated: 517.9176, found: 517.9311 (17%, $[M-H-2CO]^-$), calculated: 489.9227, found: 489.9363 (6%, $[M-H-3CO]^-$), calculated: 461.9277, found: 461.9404 (6%, $[M-H-4CO]^-$).

Compound 13: UV–Vis $\lambda_{max}(CH_2Cl_2)$/nm 350 (ε/dm^3 mol^{-1} cm^{-1} 18,940). **FT-IR** ν_{CO}(hexane)/cm^{-1} 2063 w ($A_1^{(1)}$), 1973*vw* (B_1), 1936s (E and $A_1^{(2)}$). **^{1}H NMR** δ^1H(400.13 MHz; $CDCl_3$; Me_4Si) 6.82 (2 H, s, H4), 3.96 (6 H, s, CH_3), 3.35 (6 H, s, CH_3). **^{13}C NMR** δ^{13}C(75.468 MHz; $CDCl_3$; Me_4Si) 249.3 (C_{carb}), 203.6 (CO_{trans}), 198.1 (CO_{cis}), 155.9 (C5), 110.3 (C4), 138.1 and 137.8 (C3 and C2), 54.0 and 45.7 (CH_3). **ESI-MS** *m/z*($C_{24}H_{14}N_2O_{10}S_3W_2$, 954.25 g/mol) calculated: 952.8751, found: 952.8868 (18%, $[M-H]^-$), calcu-

lated: 924.8802, found: 924.8928 (7%, $[M-H-CO]^-$), calculated: 896.8853, found: 896.8961 (3%, $[M-H-2CO]^-$), calculated: 868.8904, found: 868.9036 (6%, $[M-H-3CO]^-$).

Author agreement

All authors have seen the final version of the manuscript and approved the same before submission.

Disclosure statement

There is no financial/personal interest that could affect our objectivity.

Declaration of Competing Interest

The authors declare that they have no known competing financial interests or personal relationships that could have appeared to influence the work reported in this paper.

Acknowledgements

The authors gratefully acknowledge the National Research Foundation, South Africa (NRF 105740; NRF 105529 NRF 87788 and NRF 9772) and Sasol Technology R&D Pty. Ltd. (South Africa) for financial support.

Appendix A. Supplementary data

Supplementary data to this article (compound information from chromatographic separation, 2D-NMR spectra, crystallographic data and solid state packing) can be found online at ###.

CCDC 2009041−2009047 contain the supplementary crystallographic data for this paper. These data can be obtained free of charge via www.ccdc.cam.ac.uk/data_request/cif, or by emailing data_request@ccdc.cam.ac.uk, or by contacting The Cambridge Crystallographic Data Centre, 12 Union Road, Cambridge CB2 1EZ, UK; fax: +44 1223 336033.

Supplementary materials

Supplementary material associated with this article can be found, in the online version, at doi:10.1016/j.jorganchem.2020.121466.

References

[1] P. Li, Y. Cui, C. Song, H. Zhang, RSC Adv. 5 (62) (2015) 50212–50222.
[2] W. Jiang, Y. Li, Z. Wang, Chem. Soc. Rev. 42 (14) (2013) 6113–6127.
[3] V.G. Nenajdenko, D.V. Gribkov, V.V. Sumerin, E.S. Balenkova, Synthesis (Stuttg) 1 (1) (2003) 124–128.
[4] T. Ozturk, E. Ertas, O. Mert, Tetrahedron 61 (47) (2005) 11055–11077.
[5] H. Wang, Y. Wang, Z. Wang, Z. Wang, D. Zhao, C. Zhao, Faming Zhuanli Shenqing Gongkai Shuomingshu (2009) CN 101343279 A 20090114.
[6] S. Okada, K. Yamada, J. Mol. Struct. 1037 (2013) 256–263.
[7] G.M. Tsivgoulis, J.-M. Lehn, Angew. Chem. Int. Ed. Engl. 34 (10) (1995) 1119–1122.
[8] M.J. Janssen, F. De Jong, J. Org. Chem. 36 (12) (1971) 1645–1648.
[9] F. De Jong, M.J. Janssen, J. Org. Chem. 36 (14) (1971) 1998–2000.
[10] W.J. Archer, R. Taylor, J. Chem. Soc. Perkin Trans. 2 (3) (1982) 295–299.
[11] W.J. Archer, R. Taylor, J. Chem. Soc. Perkin Trans. 2 (3) (1982) 301.
[12] M. Landman, H. Görls, S. Lotz, J. Organomet. Chem. (2001) 617–618 280–287.
[13] M. Landman, H. Görls, S. Lotz, Z. Anorg. Allg. Chem. 628 (9–10) (2002) 2037–2043.
[14] S. Lotz, C. Crause, A.J. Olivier, D.C. Liles, H. Görls, M. Landman, D.I. Bezuidenhout, Dalton Trans. 4 (2009) 697–710.
[15] D.I. Bezuidenhout, S. Lotz, D.C. Liles, B. van der Westhuizen, Coord. Chem. Rev. 256 (5–8) (2012) 479–524.
[16] F. Allared, J. Hellberg, T. Remonen, Tetrahedron Lett. 43 (8) (2002) 1553–1554.
[17] S. Lotz, N.A. van Jaarsveld, D.C. Liles, C. Crause, H. Görls, Y.M. Terblans, Organometallics 31 (15) (2012) 5371–5383.
[18] K. Chernichenko, N. Emelyanov, I. Gridnev, V.G. Nenajdenko, Tetrahedron 67 (36) (2011) 6812–6818.
[19] Z. Wang, C. Zhao, D. Zhao, C. Li, J. Zhang, H. Wang, Tetrahedron 66 (12) (2010) 2168–2174.
[20] J.A. Connor, E.M. Jones, G.K. McEwen, M.K. Lloyd, J.A. McCleverty, J. Chem. Soc. Dalton Trans. 12 (1972) 1246.
[21] Z. Lamprecht, N.A. van Jaarsveld, D.I. Bezuidenhout, D.C. Liles, S. Lotz, Dalton Trans. 44 (44) (2015) 19218–19231.
[22] Z. Lamprecht, M.M. Moeng, D.C. Liles, S. Lotz, D.I. Bezuidenhout, Polyhedron 158 (2019) 193–207.
[23] Z. Lamprecht, S.G. Radhakrishnan, A. Hildebrandt, H. Lang, D.C. Liles, N. Weststrate, S. Lotz, D.I. Bezuidenhout, Dalton Trans. 46 (40) (2017) 13983–13993.
[24] D.M. Adams, Metal-Ligand and Related Vibrations, Edward Arnold Publishers Ltd, London, 1967.
[25] R.M. Silverstein, G. Clayton Bassler, T.C. Morris, Spectrometric Identification of Organic Compounds, third ed., John Wiley & Sons, Inc., 1980.
[26] O.S. Mills, A.D. Redhouse, J. Chem. Soc. (1968) 642–647.
[27] G. Huttner, B. Krieg, Chem. Ber. 105 (1) (1972) 67–81.
[28] U. Schubert, Organometallics 1 (8) (1982) 1085–1088.
[29] D.M. Andrada, M.E. Zoloff Michoff, I. Fernández, A.M. Granados, M.A. Sierra, Organometallics 26 (24) (2007) 5854–5858.
[30] Z. Lamprecht, MSc. Dissertation, University of Pretoria, 2015.
[31] F. Grevels, J. Jacke, W.E. Klotzbücher, F. Mark, V. Skibbe, K. Schaffner, K. Angermund, C. Krüger, C.W. Lehmann, S. Özkar, Organometallics 18 (17) (1999) 3278–3293.
[32] V.L. Deringer, A. Wang, J. George, R. Dronskowski, U. Englert, Dalton Trans. 45 (35) (2016) 13680–13685.
[33] H. Meerwein, Org. Synth. 46 (1966) 113–115.
[34] APEX3, (including SAINT and SADABS), BrukerAXS Inc., Madison, WI, 2016.
[35] Rigaku Oxford Diffraction, Rigaku Corporation, Oxford, UK, 2018.
[36] G.M. Sheldrick, Acta Crystallogr. Sect. A Found. Adv. 71 (1) (2015) 3–8.
[37] G.M. Sheldrick, Acta Crystallogr. Sect. C Struct. Chem. 71 (1) (2015) 3–8.